

# Polarizabilities of the $\text{Mg}^+$ and $\text{Si}^{3+}$ ions

J. Mitroy

*School of Engineering, Charles Darwin University, Darwin NT 0909, Australia*

M. S. Safronova

*Department of Physics and Astronomy,*

*University of Delaware, Newark, Delaware 19716-2593, USA*

(Dated: November 3, 2008)

## Abstract

A polarization analysis of the fine-structure intervals for the  $n = 17$  Rydberg states of Mg and the  $n = 29$  states of  $\text{Si}^{2+}$  is performed. The coefficients of all terms in the polarization expansion up to  $r^{-8}$  were computed using a semi-empirical single electron analysis combined with the relativistic all-order single-double method (MBPT-SD) which includes all single-double excitations from the Dirac-Fock wave functions to all orders of perturbation theory. The revised analysis yields dipole polarizabilities of  $\alpha_1 = 35.04(3)$  a.u. for  $\text{Mg}^+$  and  $\alpha_1 = 7.433(25)$  a.u. for  $\text{Si}^{3+}$ , values only marginally larger than those obtained in a previous analysis (E. L. Snow and S. R. Lundeen (2007) Phys. Rev. A **75** 062512, *ibid* (2008) **77** 052501). The polarizabilities are used to make estimates of the multiplet strength for the resonant transition for both ions. The revised analysis did see significant changes in the slopes of the polarization plots. The dipole polarizabilities from the MBPT-SD calculation, namely 35.05(12) a.u. and 7.419(16) a.u., are within 0.3% of the revised experimental values.

PACS numbers: 31.15.ap, 31.15.ag, 31.15.am, 31.15.V-

## I. INTRODUCTION

Resonant excitation Stark ionization spectroscopy (RESIS) [1] is a versatile and powerful method for studying Rydberg states of atoms and ions. One of the primary applications is the determination of deviations from the pure hydrogenic values of the binding energies. Polarization interactions between the core and the Rydberg electrons lead to the effective potential [1, 2, 3]

$$V_{\text{pol}} = -\frac{C_4}{r^4} - \frac{C_6}{r^6} - \frac{C_7}{r^7} - \frac{C_8}{r^8} - \frac{C_{8L}L(L+1)}{r^8} + \dots \quad (1)$$

This functional form has been applied to the analysis of the fine-structure spectrum of the Rydberg states of neutral Mg and  $\text{Si}^{2+}$  resulting in precise estimates of the dipole polarizabilities of the sodium-like  $\text{Mg}^+$  and  $\text{Si}^{3+}$  ground states [4, 5, 6]. The  $\text{Mg}^+$  polarizability was 35.00(5) a.u. [6] and the  $\text{Si}^{3+}$  polarizability was 7.426(12) a.u. [5]. Analysis of the spectrum has also given information about the quadrupole polarizabilities.

One area of uncertainty in the analysis is the contribution of the higher-order terms in the polarization expansion. Using theoretical estimates of  $C_7$  and  $C_{8L}$  to constrain the analysis has proved essential in obtaining values of the quadrupole polarizability that are even remotely close with theoretical estimates [5, 6]. However, some of the high order terms that contribute to Eq. (1) were omitted from the analysis of the experimental data.

This limitation is rectified in the present work which uses two different theoretical techniques to determine values of all the terms in Eq. (1). One technique supplements the Hartree-Fock core potential with a semi-empirical polarization potential and effectively solves a one-electron Schrodinger equation to determine the excitation spectrum for the valence electron [7, 8, 9]. The other method used is the relativistic all-order single-double method where all single and double excitations of the Dirac-Fock (DF) wave function are included to all orders of many-body perturbation theory (MBPT) [10, 11, 12]. We note in passing that there has been a recent configuration interaction (CI) calculation of the polarizabilities of the  $\text{Mg}^+$  and  $\text{Si}^{3+}$  ground states [13].

The current work has implications that go beyond the analysis of the RESIS experiments of the Lundeen group. One of the most active area in physics at present is the development of new atomic clocks based on groups of neutral atoms in optical lattices [14, 15, 16] or single atomic ions [14, 17]. These clocks have the potential to exceed the precision of

the existing cesium microwave standard [18]. For many of these clocks the single largest source of systematic error is the black-body radiation shift (BBR) [19, 20, 21, 22, 23]. The BBR shift to first order is proportional to the difference in polarizabilities of the two states involved in the clock transition. Many estimates of the relevant polarizabilities are determined by theoretical calculations [24, 25, 26]. Comparisons of existing techniques to calculate polarizabilities with high quality experiments will ultimately help constrain the uncertainties associated with the BBR shift.

## II. THE POLARIZATION EXPANSION

In this section the definitions of the various terms in the polarization potential are given following the analysis of Drachman [2, 3]. The notation of Lundeen [1, 5] is adopted.

The leading term,  $C_4$  is half the size of the static dipole polarizability,

$$C_4 = \frac{\alpha_1}{2} . \quad (2)$$

The dipole polarizability is defined as

$$\alpha_1 = \sum_n \frac{f_{gn}^{(1)}}{(\Delta E_{gn})^2} . \quad (3)$$

where  $f_{gn}^{(k)}$  is the absorption oscillator strength for a dipole transition from state  $g$  to state  $n$ . The absorption oscillator strength for a multi-pole transition from  $g \rightarrow n$ , with an energy difference of  $\Delta E_{ng} = E_g - E_n$ , is defined as

$$f_{gn}^{(k)} = \frac{2|\langle \psi_g; L_g \parallel r^k \mathbf{C}^k(\hat{\mathbf{r}}) \parallel \psi_n; L_n \rangle|^2 \Delta E_{ng}}{(2k+1)(2L_g+1)} . \quad (4)$$

In this expression,  $L_g$  is the orbital angular momentum of the initial state while  $k$  is the polarity of the transition. In a  $J$ -representation, the oscillator strength becomes

$$f_{gn}^{(k)} = \frac{2|\langle \psi_g; J_g \parallel r^k \mathbf{C}^k(\hat{\mathbf{r}}) \parallel \psi_n; J_n \rangle|^2 \Delta E_{ng}}{(2k+1)(2J_g+1)} . \quad (5)$$

The next term,  $C_6$ , is composed of two separate terms

$$C_6 = \frac{\alpha_2 - 6\beta_1}{2} . \quad (6)$$

The quadrupole polarizability,  $\alpha_2$  is computed as

$$\alpha_2 = \sum_n \frac{f_{gn}^{(2)}}{(\Delta E_{gn})^2} . \quad (7)$$

The second term in Eq. (6) is the non-adiabatic dipole polarizability. It is defined as

$$\beta_1 = \sum \frac{f_{gn}^{(1)}}{2(\Delta E_{gn})^3} . \quad (8)$$

The  $r^{-7}$  term,  $C_7$  also comes in two parts, namely

$$C_7 = -\frac{(\alpha_{112} + 3.2q\gamma_1)}{2} . \quad (9)$$

The  $\gamma_1$  is a higher-order non-adiabatic term

$$\gamma_1 = \sum \frac{f_{gn}^{(1)}}{4(\Delta E_{gn})^4} . \quad (10)$$

while  $q$  is the charge on the core. The dipole-dipole-quadrupole polarizability,  $\alpha_{112}$  arises from third order in perturbation theory. It is derived from the matrix element [2, 5, 27]

$$\begin{aligned} \frac{\alpha_{112}}{2R^7} &= \sum_{k_1 k_2 k_3} \sum_{n_a n_b} \frac{\langle \psi_g; 0 | V^{k_1} | \psi_{n_a}; L_a \rangle}{\Delta E_{n_g n_a} \Delta E_{n_b n_a}} \\ &\times \langle \psi_{n_a}; L_a | V^{k_2} | \psi_{n_b}; L_b \rangle \langle \psi_{n_b}; L_b | V^{k_3} | \psi_g; 0 \rangle . \end{aligned} \quad (11)$$

where  $V^k = \mathbf{C}^k(\hat{\mathbf{r}}) \cdot \mathbf{C}^k(\hat{\mathbf{R}}) r^k / R^{K+1}$ . The sum of the multipole orders must obey  $k_1 + k_2 + k_3 = 4$ . Quite a few terms contribute to  $C_8$

$$C_8 = \frac{\alpha_3 - \beta_2 - \alpha_1 \beta_1 + \alpha_{1111} + 72\gamma_1}{2} . \quad (12)$$

The octupole polarizability,  $\alpha_3$  is computed as

$$\alpha_3 = \sum \frac{f_{gn}^{(3)}}{(\Delta E_{gn})^2} . \quad (13)$$

The  $\beta_2$  comes from the non-adiabatic part of the quadrupole polarizability, it is

$$\beta_2 = \sum \frac{f_{gn}^{(2)}}{2(\Delta E_{gn})^3} . \quad (14)$$

The fourth-order term,  $\alpha_{1111}$  is related to the hyper-polarizability [28, 29]. It is defined as

$$\begin{aligned} \frac{\alpha_{1111}}{2R^8} &= \sum_{n_a n_b n_c} \frac{\langle \psi_{n_g}; 0 | V^1 | \psi_{n_a}; L_a \rangle}{\Delta E_{ga} \Delta E_{gb} \Delta E_{gc}} \\ &\times \langle \psi_{n_a}; L_a | V^1 | \psi_{n_b}; L_b \rangle \langle \psi_{n_b}; L_b | V^1 | \psi_{n_c}; L_c \rangle \\ &\times \langle \psi_{n_c}; L_c | V^1 | \psi_g; 0 \rangle . \end{aligned} \quad (15)$$

The final term,  $C_{8L}$  is non-adiabatic in origin and defined

$$C_{8L} = \frac{18\gamma_1}{5} . \quad (16)$$

### III. STRUCTURE MODELS FOR $\text{Mg}^+$ AND $\text{Si}^{3+}$

#### A. Semi-empirical method

The semi-empirical wave functions and transition operator expectation values were computed by diagonalizing the semi-empirical Hamiltonian [8, 30, 31, 32, 33] in a large mixed Laguerre type orbital (LTO) and Slater type orbital (STO) basis set [30]. We first discuss  $\text{Si}^{3+}$  and then mention  $\text{Mg}^+$ .

The initial step was to perform a Hartree-Fock (HF) calculation to define the core. The present calculation can be regarded as HF plus core polarization (HFCP). The calculation of the  $\text{Si}^{3+}$  ground state was done in a STO basis [34]. The core wave functions were then frozen, giving the working Hamiltonian for the valence electron

$$H = -\frac{1}{2}\nabla^2 + V_{\text{dir}}(\mathbf{r}) + V_{\text{exc}}(\mathbf{r}) + V_{\text{p}}(\mathbf{r}) . \quad (17)$$

The direct and exchange interactions,  $V_{\text{dir}}$  and  $V_{\text{exc}}$ , of the valence electron with the HF core were calculated exactly. The  $\ell$ -dependent polarization potential,  $V_{\text{p}}$ , was semi-empirical in nature with the functional form

$$V_{\text{p}}(\mathbf{r}) = -\sum_{\ell m} \frac{\alpha_d g_{\ell}^2(r)}{2r^4} |\ell m\rangle \langle \ell m|. \quad (18)$$

The coefficient,  $\alpha_d$  is the static dipole polarizability of the core and  $g_{\ell}^2(r) = 1 - \exp(-r^6/\rho_{\ell}^6)$  is a cutoff function designed to make the polarization potential finite at the origin. The cutoff parameters,  $\rho_{\ell}$  were tuned to reproduce the binding energies of the  $ns$  ground state and the  $np$ ,  $nd$  and  $nf$  excited states. The dipole polarizability for  $\text{Si}^{4+}$  was chosen as  $\alpha_d = 0.1624$  a.u. [30, 35]. The cutoff parameters for  $\ell = 0 \rightarrow 3$  were 0.7473, 0.8200, 1.022 and 0.900  $a_0$  respectively. The parameters for  $\ell > 3$  were set to  $\rho_3$ . The energies of the states with  $\ell \geq 1$  were tuned to the statistical average of their respective spin-orbit doublets. The Hamiltonian was diagonalized in a very large orbital basis with about 50 Laguerre type orbitals for each  $\ell$ -value. The oscillator strengths (and other multi-pole expectation values) were computed with operators that included polarization corrections [30, 31, 36, 37, 38]. The quadrupole core polarizability was chosen as 0.1021 a.u. [35] while the octupole polarizability was set to zero. The cutoff parameter for the polarization correction to the transition operator was fixed at 0.864  $a_0$  (the average of  $\rho_0$ ,  $\rho_1$ ,  $\rho_2$  and  $\rho_3$ ).

It is worth emphasizing that model potential is based on a realistic wave function and the direct and exchange interactions with the core were computed without approximation from the HF wave function. Only the core polarization potential is described with an empirical potential.

The overall methodology of the  $\text{Mg}^+$  calculation is the same as that for  $\text{Si}^{3+}$  and many of the details have been given previously [25]. The core dipole polarizabilities were  $\alpha_d = 0.4814$  a.u. [7, 30] and  $\alpha_q = 0.5183$  a.u. for  $\text{Mg}^{2+}$  [30, 35]. The octupole polarizability was set to zero. The  $\text{Mg}^{2+}$  cutoff parameters for  $\ell = 0 \rightarrow 3$  were 1.1795, 1.302, 1.442, and 1.520  $a_0$  respectively. The cutoff parameter for evaluation of transition multipole matrix elements was 1.361  $a_0$ .

The HF-CP calculations of the polarizabilities utilized the list of multipole matrix elements and energies resulting from the diagonalization of the effective Hamiltonian. These were directly used in the evaluation of the polarizability sum rules.

## B. The all-order method

In the relativistic all-order method including single, double, and valence triple excitations, the wave function is represented as an expansion

$$\begin{aligned} |\Psi_v\rangle = & \left[ 1 + \sum_{ma} \rho_{ma} a_m^\dagger a_a + \frac{1}{2} \sum_{mnab} \rho_{mnab} a_m^\dagger a_n^\dagger a_b a_a + \right. \\ & + \sum_{m \neq v} \rho_{mv} a_m^\dagger a_v + \sum_{mna} \rho_{mnva} a_m^\dagger a_n^\dagger a_a a_v \\ & \left. + \frac{1}{6} \sum_{mnrab} \rho_{mnrab} a_m^\dagger a_n^\dagger a_r^\dagger a_b a_a a_v \right] |\Phi_v\rangle, \end{aligned} \quad (19)$$

where  $\Phi_v$  is the lowest-order atomic state wave function, which is taken to be the *frozen-core* DF wave function of a state  $v$  in our calculations. In second quantization, the lowest-order atomic state function is written as

$$|\Phi_v\rangle = a_v^\dagger |0_C\rangle,$$

where  $|0_C\rangle$  represents the DF wave function of the closed core. In Eq. (19),  $a_i^\dagger$  and  $a_i$  are creation and annihilation operators, respectively. Indices at the beginning of the alphabet,  $a, b, \dots$ , refer to occupied core states, those in the middle of the alphabet  $m, n, \dots$ , refer to

excited states, and index  $v$  designates the valence orbital. We refer to  $\rho_{ma}$ ,  $\rho_{mv}$  as single core and valence excitation coefficients and to  $\rho_{mnab}$  and  $\rho_{mnva}$  as double core and valence excitation coefficients, respectively. The quantities  $\rho_{mnrwab}$  are valence triple excitation coefficients and are included perturbatively where necessary as described in Ref. [11].

To derive the equations for the excitation coefficients, the wave function  $\Psi_v$ , given by Eq. (19), is substituted into the many-body Schrödinger equation

$$H|\Psi_v\rangle = E|\Psi_v\rangle, \quad (20)$$

where the Hamiltonian  $H$  is the relativistic *no-pair* Hamiltonian [39]. This can be expressed in second quantization as

$$H = \sum_i \epsilon_i : a_i^\dagger a_i : + \frac{1}{2} \sum_{ijkl} g_{ijkl} : a_i^\dagger a_j^\dagger a_l a_k :, \quad (21)$$

where  $\epsilon_i$  is the DF energy for the state  $i$ ,  $g_{ijkl}$  are the two-body Coulomb integrals, and  $: :$  indicates normal order of the operators with respect to the closed core. In the *no-pair* Hamiltonian, the contributions from negative-energy (positron) states are omitted.

The resulting all-order equations for the excitation coefficients  $\rho_{ma}$ ,  $\rho_{mv}$ ,  $\rho_{mnab}$ , and  $\rho_{mnva}$  are solved iteratively with a finite basis set, and the correlation energy is used as a convergence parameter. As a result, the series of correlation correction terms included in the SD (or SDpT) approach are included to all orders of many-body perturbation theory (MBPT) as an additional MBPT order is picked up at each iteration. The basis set is defined in a spherical cavity on a non-linear grid and consists of single-particle basis states which are linear combinations of  $B$ -splines [40]. The contribution from the Breit interaction is negligible for all matrix elements considered in this work.

The matrix element of any one-body operator  $Z$  in the all-order method is obtained as

$$Z_{vw} = \frac{\langle \Psi_v | Z | \Psi_w \rangle}{\sqrt{\langle \Psi_v | \Psi_v \rangle \langle \Psi_w | \Psi_w \rangle}}. \quad (22)$$

The numerator of the resulting expression consists of the sum of the DF matrix element  $z_{wv}$  and twenty other terms  $Z^{(k)}$ ,  $k = a \cdots t$ . These terms are linear or quadratic functions of the excitation coefficients  $\rho_{ma}$ ,  $\rho_{mv}$ ,  $\rho_{mnab}$ , and  $\rho_{mnva}$ . More details on the SD and SDpT methods and their applications can be found in Refs. [11, 12, 41]. We find that the contribution of triple excitations is small for the atomic properties considered in this work. So the SD approximation is used for most transitions.

The  $B$ -spline basis used in the calculations included  $N = 50$  basis orbitals for each angular momentum within a cavity radius of  $R_0 = 100 a_0$  for  $\text{Mg}^+$  and  $R_0 = 80 a_0$  for  $\text{Si}^{3+}$ . Such large cavities are needed to fit highly-excited states such as  $8h$  needed for the  $3d$  octupole polarizability calculations. The single-double (SD) all-order method yielded results for the primary  $ns - np_j$  electric-dipole matrix elements of alkali-metal atoms that are in agreement with experiment to 0.1%-0.5% [11]. We refer to the results obtained with this method as MBPT-SD in the subsequent text and Tables.

Since the all-order calculations are carried out with a finite basis set, the sums given by Eqs. (3) - (13) run up to the number of the basis set orbitals ( $N = 50$ ) for each partial wave. For consistency, the same  $B$ -spline basis is used in all calculations of the same system (e.g.  $\text{Mg}^+$  or  $\text{Si}^{3+}$ ).

The calculation of the polarizabilities for the MBPT-SD uses slightly different procedures to include different parts of the polarizability sum rules. The all-order matrix elements were combined with the experimental energies for excited states with  $n \leq 6$  for  $\beta = ns, np_{1/2}, np_{3/2}, nd_{3/2}, nd_{5/2}$ ,  $n \leq 7$  for  $\beta = nf_{5/2}, nf_{7/2}$ , and  $n \leq 8$  for  $\beta = ng_{7/2}, ng_{9/2}, nh_{9/2}, nh_{11/2}$ . The remaining matrix elements and energies were calculated in the DF approximation, with the exception of the  $3s$  dipole polarizability, where the remaining matrix elements were calculated using random-phase approximation (RPA) [42] for the purpose of error evaluation. These remainder contributions are small for dipole polarizabilities (0.2-5%) but increase in relative size for the quadrupole (0.3-10%) and octupole (4-20%) polarizabilities. An extra correction was introduced to the remainder contribution for octupole polarizabilities. First, the accuracy of the DF calculations was estimated from a comparison of the DF and all-order results for the few first terms. Then, these estimates were used to adjust the remainder. The improvement of the DF results for states with higher  $n$  was also taken into account. The size of this extra correction ranged from 0.9% to 6% of the tail contributions as the accuracy of the DF approximation for these highly-excited states is rather high. The net effect of this scaling was usually to reduce the octupole polarizabilities by an amount of about 0.5-1.5%.

The core contribution was calculated in the RPA [35] with the exception of the dipole polarizability for the  $\text{Mg}^{2+}$  core. In this case the polarizability of  $\alpha_d = 0.4814$  a.u. was taken from a pseudo-natural orbital CI type calculation [7, 30]. A small  $\alpha_{cv}$  correction for the dipole polarizability that compensates for excitations from the core to occupied valence



states was also determined using RPA matrix elements and DF energies. The relative impact of the core polarizability was at least a factor of two smaller for the quadrupole polarizability.

## IV. GROUND AND EXCITED PROPERTIES

### A. The energy levels

The binding energies of the low-lying states of the  $\text{Mg}^+$  and  $\text{Si}^{3+}$  are tabulated and compared with experiment in Table I. The agreement between the HFCEP energies and the experimental energies is generally of order  $10^{-4}$  Hartree. When the  $\rho_\ell$  cutoff parameters are tuned to the lowest state of each symmetry the tendency is for higher states of the same symmetry to be slightly under-bound. The MBPT-SD binding energies generally agree with experiment to better than  $10^{-4}$  Hartree. The MBPT-SD binding energies do not suffer any systematic tendency to either underbind or overbind as  $n$  increases.

### B. Line strengths

Table II lists the line strengths for the resonant transitions of Na,  $\text{Mg}^+$ ,  $\text{Al}^{2+}$  and  $\text{Si}^{3+}$ . All line strengths here and in the text below are given in a.u.. The HFCEP values for sodium are from calculations previously reported in Ref. [58] while the values for  $\text{Al}^{2+}$  were taken from a calculation very similar in style and execution to the present calculations [59]. The MBPT-SD line strengths for Na and  $\text{Al}^{2+}$  were taken from Ref. [10]. Values from the extensive tabulation of dipole line strengths using a  $B$ -spline non-orthogonal configuration interaction with the Breit interaction (BSR-CI) [60] are also listed. The HFCEP line strengths were computed from a common multiplet strength by multiplying by the appropriate recoupling coefficients [61].

The comparisons for the resonant  $3s \rightarrow 3p$  transition reveal that the HFCEP line strengths are the smallest, the BSR-CI line strengths are the largest and the MBPT-SD line strengths are intermediate between these two calculations. The MBPT-SD dipole strengths are closer to HFCEP for Na,  $\text{Mg}^+$  and  $\text{Al}^{2+}$  and about half-way between HFCEP and BSR-CI for  $\text{Si}^{3+}$ . The total variation between the three different calculations is about 1%. The most precise experiments performed on the Na-like iso-electronic series of atoms(ions) are those performed on sodium itself [44, 45, 46, 47, 48]. The experimental line strengths for sodium are in better

agreement with the MBPT-SD and HFCP line strengths than they are with the BSR-CI line strengths.

There have been two precision measurements of the  $3s \rightarrow 3p$  transition rate for  $\text{Mg}^+$ . The experiment of Ansbacher *et al.* [49] gave slightly larger line strengths which agree best with the BSR-CI values. However, the most recent trapped ion experiment [50] gave a  $3s_{1/2} \rightarrow 3p_{3/2}$  line strength of 11.24(6) that is in better agreement with the HFCP/MBPT-SD line strengths.

Table III lists the line strengths for a number of other dipole transitions for  $\text{Mg}^+$  and  $\text{Si}^{3+}$ . The line strengths for the quadrupole  $3s \rightarrow nd$  transitions are also listed due to their importance in the determination of the quadrupole polarizabilities.

The  $3p \rightarrow 3d$  transition is the strongest transition emanating from the  $3p$  level. The comparison between the three calculations exhibits a pattern similar to that of the resonant transition. The HFCP line strengths are smallest, the BSR-CI line strengths are the largest, and the MBPT-SD line strengths lie somewhere between these two calculations.

The astrophysically important  $\text{Mg}^+$   $3s \rightarrow 4p$  transition has a very small dipole strength. It is close to the Cooper minimum [62] in the  $3s \rightarrow np$  matrix elements and therefore is more sensitive to the slightly different energies between the spin-orbit doublet. This caused the ratio of line strengths for the  $4p_{1/2}$  and  $4p_{3/2}$  transitions to deviate from the expected value of 2. The MBPT-SD branching ratio of 1.76 agrees with the recent experimental values of 1.74(6) [63] and 1.82(8) [63, 64]. The HFCP multiplet strength of 0.00752 and the MBPT-SD multiplet strength of 0.00721 are about 5-10% smaller than the recent experimental estimates of 0.00793(26) [63] and 0.00775(50) [63, 64].

There is also a deviation from the ratio of 2 for the  $3s \rightarrow 4p_{1/2,3/2}$  transitions of  $\text{Si}^{3+}$ . However, in this case the deviation is smaller. Ratios of line strengths for the stronger transitions are much closer to values expected from purely angular recoupling considerations. The  $3p_{3/2} : 3p_{1/2}$  ratio for  $\text{Si}^{3+}$  was 2.002. The  $3p \rightarrow 4s$  transition ratio has a slight deviation from 2, the MBPT-SD calculations giving 2.015 for  $\text{Mg}^+$  and 2.006 for  $\text{Si}^{3+}$  (the BSR-CI ratios are similar).

The better than 0.5% agreement between the model potential and MBPT-SD line strengths for strong transitions is consistent with previous comparisons. The general level of agreement between calculations with a semi-empirical core potential and more sophisticated ab-initio approaches for properties such as oscillator strengths, polarizabilities and

dispersion coefficients has generally been very good [30, 65, 66, 67]. There was a tendency for the agreement between the HFCP and MBPT-SD line strengths to degrade slightly from  $\text{Mg}^+$  and  $\text{Si}^{3+}$ . This is probably due to the increased importance of relativistic effects as the nuclear charge increases.

### C. Polarizabilities

The polarizabilities of the  $3s$ ,  $3p$  and  $3d$  levels of  $\text{Mg}^+$  and  $\text{Si}^{3+}$  are listed in Table IV. Tensor polarizabilities are also determined for the  $3p$  and  $3d$  levels. Definitions of the tensor polarizability,  $\alpha_{1,2JJ}$ , in terms of oscillator strength sum rules can be found in Refs. [68] and [69].

Table V gives a short breakdown of the contributions of different terms to the dipole polarizability while Table VI gives the breakdown for the quadrupole polarizability. The  $3s \rightarrow \varepsilon p(d)$  contribution represents anything over  $n = 6$  and can be regarded as a mix of some higher discrete states as well as the pseudo-continuum. Polarizabilities for the  $\text{Mg}^+$  and  $\text{Si}^{3+}$  ground states from other sources are also listed in Table V and VI. The HFCP  $\text{Mg}^+$  polarizability is marginally smaller than that reported previously [25] since the present evaluation includes a small core-valence correction.

The very good agreement between the HFCP and MBPT-SD polarizabilities is a notable feature of Table IV. None of the static polarizabilities differ by more than 0.5% with the exception being the  $\alpha_2$  of the  $\text{Mg}^+$   $3d$  state. Here the difference is caused by the very small  $\Delta E_{3d-4s}$  energy difference which is sensitive to small errors in the HFCP energies. The relative difference between some of the tensor polarizabilities is larger, but this is due to cancellations between the component sum rules that are combined to give the tensor polarizability.

A recent CI calculation of the  $\text{Mg}^+$  and  $\text{Si}^{3+}$  ground state dipole polarizabilities [13] gave polarizabilities that were 1-2% larger than the HFCP/MBPT-SD polarizabilities. The more recent relativistic coupled-cluster (RCC) calculation [57] gave polarizabilities that were compatible with the present values.

The dipole polarizabilities for both  $\text{Mg}^+$  and  $\text{Si}^{3+}$  are dominated by the resonant oscillator strength. For  $\text{Mg}^+$  one finds that 98.3% of  $\alpha_1$  arises from the  $3s \rightarrow 3p$  transition. For  $\text{Si}^{3+}$  the contribution is smaller but still substantial at 96.7%. The non-adiabatic dipole

polarizabilities are even more dominated by the contribution from the resonant transition. One finds that 99.9% of  $\beta_1$  and 99.99% of  $\gamma_1$  for  $\text{Mg}^+$  come from this transition. The proportions for the  $\text{Si}^{3+}$   $\beta_1$  and  $\gamma_1$  are 99.6% and 99.92% respectively.

The quadrupole polarizabilities are also dominated by a single transition. Table VI shows that the  $3s \rightarrow 3d$  excitation constitutes at least 95% of  $\alpha_2$  for both  $\text{Mg}^+$  and  $\text{Si}^{3+}$ .

The calculation of the  $\alpha_{112}$  and  $\alpha_{1111}$  polarizabilities was a composite calculation using both MBPT-SD and HFCP matrix elements. The HFCP calculation automatically generates a file containing matrix elements between every state included in the basis. The more computationally intensive MBPT-SD calculation was used for the largest and most important matrix elements. The HFCP matrix elements for the  $3s \rightarrow 3p$ ,  $3p \rightarrow 3d$ ,  $3s \rightarrow 3d$  and  $3p \rightarrow 4s$  transitions were replaced by  $J$  weighted averages of the equivalent MBPT-SD matrix elements. This procedure combines the higher accuracy of the MBPT-SD calculation with the computational convenience of the HFCP calculation. The justification for this procedure is that the predominant contribution to the polarizability comes from the low-lying transitions. The resulting polarizabilities are listed in Table VII. The biggest change in  $\alpha_{112}$  and  $\alpha_{1111}$  resulting from using the composite matrix element list was less than 0.3%. The  $\alpha_{112}$  and  $\alpha_{1111}$  polarizabilities did not allow for contributions from the core. The impact of the core will be small due to large energy difference involving core excitations. The relative effect of the core for  $\alpha_{112}$  and  $\alpha_{1111}$  can be expected to be about as large as the core effect in the ground state  $\alpha_1$  and  $\alpha_2$  since there are core excitations that contribute to with only one core energy in the energy denominator. For example, consider the  $\alpha_{112}$  excitation sequence of  $2p^6 3s \ ^2S^e \rightarrow 2p^5 3s 3d \ ^2P^o \rightarrow 2p^6 3d \ ^2D^e \rightarrow 2p^6 3s \ ^2S^e$ . The numerical procedures used to generate the  $\alpha_{112}$  and  $\alpha_{1111}$  polarizabilities were validated for  $\text{He}^+$ . A calculation of the  $\text{He}^+$  excitation spectrum was performed and the resulting lists of reduced matrix elements were entered into the polarizability programs. All the coefficients given by Drachman [70] were reproduced.

The polarizabilities in Table VII from the composite matrix element list could be regarded as the recommended set of polarizabilities. The MBPT-SD matrix elements are used for the dominant low-lying transitions. The HFCP matrix elements are more accurate than the RPA/DF matrix elements used for the  $3s \rightarrow \varepsilon p(d)$  remainders. The only difference between the Table VII and MBPT-SD polarizabilities occurs for  $\alpha_3$ . A relatively large part of  $\alpha_3$  comes from the higher excited states and the continuum. Accumulating a lot of small

contributions is tedious for the computationally expensive MBPT-SD, so this is done with the less accurate DF approach. In this case the HFCEP polarizability is to be preferred. It should be noted that the octupole polarizability is of minor importance in the subsequent analysis.

#### D. Error assessment

Making an a-priori assessment of the accuracy of the HFCEP polarizabilities is problematic since they are semi-empirical in nature. The error assessment for the MBPT-SD proceeds by assuming that the total contribution of fourth- and higher-order terms omitted by the SD all-order method does not exceed the contribution of already included fourth- and higher-order terms. Thus, the uncertainty of the SD matrix elements is estimated to be the difference between the SD all-order calculations and third-order results.

This procedure was applied to the  $S_{3s-3p_{1/2}}$  line strength of sodium yielding an uncertainty  $\delta S_{3s-3p_{1/2}} = 0.092$ . This uncertainty exceeds the difference between the SD line strength of 12.47 [10] and recent high precision experiments which give 12.412(16) [44, 45], and 12.435(41) [46]. A similar situation applies for the  $S_{3s-3p_{3/2}}$  line strength.

A detailed first principles evaluation of the uncertainty of the  $\text{Si}^{3+}$  static dipole polarizability has been done and the uncertainty budget is itemized in Table V. In this case, the difference between the SD line strength and third order line strength for the resonance transition was 0.082%. The uncertainties in the remaining ( $n = 4 - 6$ ) discrete transitions were of similar size. Uncertainties in the energies used in the oscillator strength sum rule can be regarded as insignificant since experimental energies were used. To estimate the accuracy of the remainder of the valence sum, the ( $n = 4 - 6$ ) calculation was repeated using RPA matrix elements and DF energies. The difference of 3% between the MBPT-SD and DF/RPA values was assessed to be the uncertainty in the  $\varepsilon p$  remainder. The good agreement between the HFCEP and DF/RPA for the non-resonant valence contribution gives additional evidence that the uncertainty estimate is realistic.

The core dipole polarizability calculated in the RPA is known to underestimate the actual core polarizability. For neon, the RPA gives  $\alpha_1 = 2.38$  a.u. [35] which is 11% smaller than the experimental value of 2.669 a.u. [71]. For  $\text{Na}^+$ , the RPA gives 0.9457 a.u. [35] while experiment gives 1.0015(15) a.u. [72]. The pseudo-natural orbital approach used for  $\text{Mg}^{2+}$

gave  $\alpha_1 = 2.67$  a.u. for Ne [73] and  $\alpha_1 = 0.9947$  a.u. for  $\text{Na}^+$  [7]. The uncertainty in the quadrupole core polarizability is based on comparisons with coupled cluster calculations for neon [74, 75]. The RPA value of 6.423 a.u. is about 12% smaller than the coupled cluster values of 7.525 a.u. [75] and 7.525 a.u. [74]. The relative uncertainties are  $\delta\alpha_1(\text{Mg}^{2+}) = 2\%$ ,  $\delta\alpha_1(\text{Si}^{4+}) = 5\%$ ,  $\delta\alpha_2(\text{Mg}^{2+}) = 12\%$ , and  $\delta\alpha_2(\text{Si}^{4+}) = 12\%$ . The core-valence correction was assigned an uncertainty of 20% based on differences between DF and RPA matrix elements. The RPA error estimates are likely to be very conservative since the uncertainty in the RPA polarizabilities is expected to decrease as the nuclear charge increases.

Combining the uncertainties in the valence and core polarizabilities for  $\text{Si}^{3+}$  gives a final uncertainty of 0.16 a.u. (or 0.22%) in the MBPT-SD  $\alpha_1$ .

The uncertainty in the  $\text{Si}^{3+}$   $\alpha_2$  listed in Table VI was evaluated with a process that was similar to the dipole polarizability. The difference between the SD line strength and third order line strength for the  $3s \rightarrow 3d_{5/2}$  transition was 0.064% (the relative uncertainty was almost the same for the transition to the  $3d_{3/2}$  state). This uncertainty is slightly smaller than that for the resonant dipole transition. This was expected since the  $3d$  electron is further away from the nucleus than the  $3p$  electron and therefore correlation-polarization corrections have less importance. Rather than do a computationally expensive analysis, the relative uncertainties in the  $(nd + \epsilon d)$  remainders were conservatively assigned to be same as for the dipole transitions. The final uncertainty was  $\delta\alpha_2 = 0.03$  a.u..

The relative uncertainties in the  $\text{Mg}^+$  polarizabilities are set in the same way as  $\text{Si}^{3+}$ . The difference between the third-order and all-order dipole line strengths for the resonance transition was 0.3%. The relative differences were larger for the  $n = 4 - 6$  transitions due to their small size. For example, the third-order/all-order comparison for the  $S_{3s-4p}$  multiplet strength gave 5%. This is consistent with the difference with the experimental multiplet strength. The uncertainties were slightly smaller for the slightly larger  $5p$  and  $6p$  transitions. However, the net contribution to the uncertainty was miniscule since the line strengths were so small. The  $3s \rightarrow \epsilon p$  uncertainty of 5% was based on differences between the HFCP and DF/RPA matrix elements.

The uncertainties in the  $\text{Mg}^+$   $\alpha_2$  polarizability are listed in Table VI and  $n = 3 - 6$  transitions were derived from the third-order/all-order comparison. The relative uncertainty in the  $3s \rightarrow 3d$  transition was 0.22%. The very good agreement between the HFCP and MBPT-SD values for these terms is further supportive of a small uncertainty for the  $n = 3 - 6$

transitions. The 7% uncertainty in the  $3d \rightarrow \varepsilon d$  remainder was based on the differences between the MBPT-SD and DF matrix elements.

The relative uncertainties in the octupole polarizabilities listed in Table VII were set to the uncertainties in the quadrupole polarizabilities. The  $nf$  orbitals are further away from the core than the  $3d$  orbitals and so the  $\alpha_2$  uncertainty serves as a convenient overestimate.

The uncertainties in the higher-order polarizabilities  $\beta_1$ ,  $\beta_2$  and  $\gamma_1$  listed in Table VII were taken to be the uncertainties in the resonant line strengths. The higher powers in the energy denominator means other transition make a negligible contribution.

The uncertainties in  $\alpha_{112}$  and  $\alpha_{1111}$  were derived from the uncertainties in the reduced matrix elements. The relative uncertainties for the most important  $3s \rightarrow 3p$ ,  $3p \rightarrow 3d$  and  $3s \rightarrow 3d$  matrix elements were simply added to give relative uncertainties for valence part of  $\alpha_{112}$  and  $\alpha_{1111}$ . The relative uncertainty resulting from the omission of core excitations was taken as the ratio of the core to total dipole polarizability and added to the  $\alpha_{112}$  and  $\alpha_{1111}$  uncertainties.

The uncertainties in  $C_6$ ,  $C_7$ ,  $C_8$  and  $C_{8L}$  were determined by combining the uncertainties of the constituent polarizabilities. The most important of these parameters is the expected slope of the polarization plot, i.e.  $\delta C_6 = \delta \alpha_2 / 2 + 3\delta \beta_1$ . For  $\text{Si}^{3+}$  we get  $\delta C_6 = 0.015 + 0.027 = 0.042$ . For  $\text{Mg}^+$  the uncertainty was  $\delta C_6 = 1.2$ .

## V. POLARIZATION ANALYSIS OF RYDBERG STATES

### A. The polarization interaction

The various polarizabilities needed for the polarization analysis are listed in Table VII. The  $C_7$ ,  $C_8$  and  $C_{8L}$  values were used to make corrections to the experimental energy intervals. The  $C_4$  value was used in computing the second-order energy shift. The transition matrix elements used in this calculation represent a synthesis of the HFCP and MBPT-SD calculations.

Estimates of  $C_7$  and  $C_{8L}$  were previously made by Snow and Lundeen [5] using MBPT-SD transition amplitudes for the lowest lying transitions. These earlier estimates are within a few percent of the present more sophisticated analysis. The Snow and Lundeen values for  $C_7$  were  $-1684(9)$  a.u. for  $\text{Mg}^+$  and  $-122(9)$  a.u. for  $\text{Si}^{3+}$ . They are a few percent smaller

than those listed in Table VII due to the omission of higher excitations from the sum rule. The Snow and Lundeen values for  $C_{8L}$  were 1170(12) a.u. for  $\text{Mg}^+$  and 60.5 a.u. for  $\text{Si}^{3+}$ .

One aspect of Table VII that is relevant to the interpretation of experiments is the importance of the non-adiabatic dipole polarizabilities. Consider  $\text{Mg}^+$  for example. The respective contributions to  $C_6$  are 78.05 a.u. from  $\alpha_2$  and  $-318.0$  a.u. from  $-6\beta_2$ . Similarly, one finds that the  $\gamma_1$  term of  $-1.6 \times 324.7$  makes up 30% of the final  $C_7$  value of  $-1727$  a.u. And finally, one finds that the  $C_8$  value of 10672 is largely due to the  $36\gamma_1$  contribution of 11689 a.u.. The degree of importance of the non-adiabatic terms scarcely diminishes for the  $\text{Si}^{3+}$  ion.

Table VIII gives the energy shifts to the  $n = 17$  levels of  $\text{Mg}^+$  and the  $n = 29$  levels of  $\text{Si}^{3+}$  using the values in Table VII. The energy shifts need  $\langle r^{-n} \rangle$  expectation values which were evaluated using the formulae of Bockasten [76].

## B. The polarization plot

Polarizabilities can be extracted from experimental data by using a polarization plot. This is based on a similar procedure that is used to determine the ionization limits of atoms [77]. The notations  $B_4$  and  $B_6$ , (instead of  $C_4$  and  $C_6$ ) are used to represent the polarization parameters extracted from the polarization plot. This is to clearly distinguish them from polarization parameters coming from atomic structure calculation. Assuming the dominant terms leading to departures from hydrogenic energies are the  $B_4$  and  $B_6$  terms, one can write

$$\frac{\Delta E}{\Delta \langle r^{-4} \rangle} = B_4 + B_6 \frac{\Delta \langle r^{-6} \rangle}{\Delta \langle r^{-4} \rangle} . \quad (23)$$

In this expression,  $\Delta E$  is the energy difference between two states of the same  $n$  but different  $L$ , while  $\Delta \langle r^{-6} \rangle$  and  $\Delta \langle r^{-4} \rangle$  are simply the differences in the radial expectations of the two states.

There are other corrections that can result in Eq. (23) departing from a purely linear form. These are relativistic energy shifts, Stark shifts due to a residual electric field, and polarization shifts due to the  $C_7$ ,  $C_8$  (and possibly higher-order) terms of Eq. (1). The energy difference between the  $(n, L)$  and  $(n, L')$  states can be written

$$\begin{aligned} \Delta E = & \Delta E_4 + \Delta E_6 + \Delta E_7 + \Delta E_8 + \Delta E_{8L} \\ & + \Delta E_{\text{rel}} + \Delta E_{\text{sec}} + \Delta E_{\text{ss}} , \end{aligned} \quad (24)$$



where  $\Delta E_n$  arises from the polarization terms of order  $\langle r^{-n} \rangle$ .

Dividing through by  $\Delta\langle r^{-4} \rangle$  and replacing  $\Delta E_6$  by  $B_6\Delta\langle r^{-6} \rangle$  gives

$$\begin{aligned} \frac{\Delta E}{\Delta\langle r^{-4} \rangle} = & B_4 + B_6 \frac{\Delta\langle r^{-6} \rangle}{\Delta\langle r^{-4} \rangle} + \frac{\Delta E_7 + \Delta E_8 + \Delta E_{8L}}{\Delta\langle r^{-4} \rangle} \\ & + \frac{\Delta E_{\text{rel}} + \Delta E_{\text{sec}} + \Delta E_{\text{ss}}}{\Delta\langle r^{-4} \rangle} . \end{aligned} \quad (25)$$

The influence of the Stark shifts, relativistic shifts, and second-order polarization correction can be incorporated into the polarization plot by simply subtracting the energy shifts. The corrected energy shift,  $\Delta E_{c1}$ , is defined as

$$\frac{\Delta E_{c1}}{\Delta\langle r^{-4} \rangle} = \frac{\Delta E_{\text{obs}}}{\Delta\langle r^{-4} \rangle} - \frac{\Delta E_{\text{rel}} + \Delta E_{\text{sec}} + \Delta E_{\text{ss}}}{\Delta\langle r^{-4} \rangle} . \quad (26)$$

An approximate expression is used for the relativistic energy correction. This is taken from the result

$$E_{\text{rel}} = -\frac{\alpha^2 Z^4}{2n^3} \left( \frac{1}{j + 1/2} - \frac{3}{4n} \right) . \quad (27)$$

The correction due to second-order effects,  $\Delta E_{\text{sec}}$ , uses the results of Drake and Swainson [78]. The Stark shift corrections use the Stark shift rates from Snow and Lundeen [5, 6] and the deduced electric field. The energy corrections due to relativistic and polarization effects for the states of  $\text{Mg}^+$  and the  $\text{Si}^{3+}$  for which RESIS data existed are listed in Table VIII.

The second corrected energy is defined by further subtracting the polarization shifts,  $\Delta E_7$ ,  $\Delta E_8$  and  $\Delta E_{8L}$ ,

$$\frac{\Delta E_{c2}}{\Delta\langle r^{-4} \rangle} = \frac{\Delta E_{c1}}{\Delta\langle r^{-4} \rangle} - \frac{\Delta E_7 + \Delta E_8 + \Delta E_{8L}}{\Delta\langle r^{-4} \rangle} . \quad (28)$$

### C. $\text{Mg}^+$

The energy splitting between adjacent  $L$  Rydberg levels is dominated by the  $C_4$  term. The next biggest term is the  $\Delta E_6$  term which is 3% of  $\Delta E_4$  for the (17,6)-(17,7) interval. The  $\Delta E_{8L}$  correction is larger than  $\Delta E_7$ . The relative impact of the higher-order corrections diminishes as  $L$  increases.

The revised analysis of the RESIS energy intervals for  $\text{Mg}^+$  was performed by subtracting the  $\Delta E_{c1}$  and  $\Delta E_{c2}$  energy corrections itemized in Table VIII from the observed energy splittings. This represents a refinement over the previous analysis by Snow and Lundeen [6] in a couple of respects. First, Snow and Lundeen did not include the  $C_8$  term since the

necessary polarizability information simply was not available. Their evaluation of  $\alpha_{112}$  only included the  $3p$  and  $3d$  states in the intermediate sums. The truncation of the sums in the  $\alpha_{112}$  calculation was justified as the correction to  $\alpha_{112}$  from a more complete evaluation was only a few percent. The impact of the  $\Delta E_8$  shift is more substantial. Table VIII shows the relative size of  $\Delta E_8$  with respect to  $\Delta E_7$  ranging from 35% to 11%.

Figure 1 shows the polarization plot for  $\text{Mg}^+$ . Linear regression was applied to the four data points with  $\Delta\langle r^{-6}\rangle/\Delta\langle r^{-4}\rangle < 0.002$ . The (17,6)-(17,7) interval was omitted from the fit because the influence of  $\Delta E_{7,8,8L}$  and  $\Delta E_{\text{sec}}$  amount to just over 50% of  $\Delta E_6$ . Visual examination of Figure 1 shows this data point lies a significant distance away from the line of best fit obtained from the four remaining points. The linear regression gave an intercept of  $B_4 = 17.522(7)$  a.u. and a slope of  $B_6 = -251.2(79)$  a.u.. The quoted uncertainties are the statistical uncertainties from the linear regression fit.

The new value of the dipole polarizability derived from the polarization plot intercept was 35.044 a.u.. This is marginally larger than the polarizability of 35.00(5) a.u. given in the original Snow and Lundeen analysis [6]. The present  $\alpha_1$  is larger because the additional corrections in the  $\Delta E_{c2}$  energies lead to a steeper polarization plot.

The slope of  $B_6 = -251.2(79)$  is slightly steeper than the Table VII recommended  $C_6$  of  $-240.1(12)$ . Using the slope of  $-251.2$  in conjunction with a  $\beta_1 = 106.0$  a.u. gives a quadrupole polarizability of  $\alpha_2 = -502.4 + 636.3 = 133.9$  a.u.. This is about 90 a.u. smaller than the polarizability of 222(54) a.u.. given by Snow and Lundeen [6]. However it is only 22 a.u. smaller than the theoretical polarizabilities of 156.1 a.u.. The uncertainty in the derived quadrupole polarizability would be  $(2 \times 7.9 + 6 \times 0.3) = 17.6$ . The RESIS and theoretical values are slightly outside their respective combined error estimates. However, the uncertainty estimate used for  $C_6$  is purely statistical in nature and does not allow higher order corrections to Eq. (23). This point is discussed in more detail later.

The relatively large change in  $\alpha_2$  from 222(54) to 134(18) a.u. was caused by the inclusion of  $\Delta E_8$ . There is a near cancellation between some of the  $\Delta E_7$  and  $\Delta E_{8L}$  energy corrections. Hence the inclusion of the  $\Delta E_8$  energy correction has a relatively large impact. For example, the sum of  $\Delta E_7$  and  $\Delta E_{8L}$  for the (17,7)-(17,8) interval was 1.473 MHz. The  $\Delta E_8$  correction was 0.851 MHz.

The derived dipole polarizability and value of  $B_6$  are not sensitive to small changes in the  $C_n$  values used for the corrections. An analysis using alternate  $C_n$  values derived

from the uncertainties detailed in Table VII was performed. This resulted in an additional uncertainty of 0.0004 a.u. in  $B_4$  and an additional uncertainty of 1.6 in  $B_6$ . These additional uncertainties were sufficiently small to ignore in subsequent analysis.

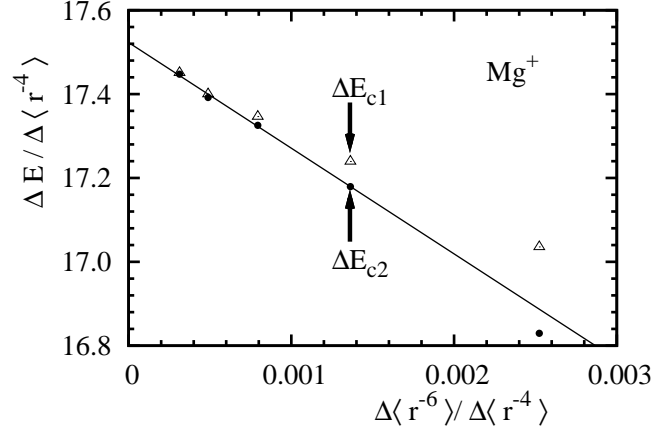


FIG. 1: The polarization plot of the fine-structure intervals of Mg for the  $n = 17$  Rydberg levels. The  $\Delta E_{c1}$  intervals are corrected for relativistic, second-order and Stark shifts. The  $\Delta E_{c2}$  intervals account for  $\langle r^{-7} \rangle$  and  $\langle r^{-8} \rangle$  shifts. The linear regression for the  $\Delta E_{c2}$  plot did not include the last point.

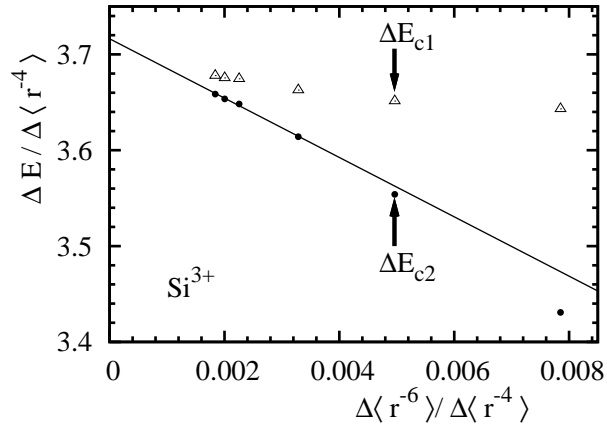


FIG. 2: The polarization plot of the fine-structure intervals of  $\text{Si}^{2+}$  for the  $n = 29$  Rydberg levels. The  $\Delta E_{c1}$  intervals are corrected for relativistic, second-order and Stark shifts. The  $\Delta E_{c2}$  intervals account for  $\langle r^{-7} \rangle$  and  $\langle r^{-8} \rangle$  shifts. The linear regression for the  $\Delta E_{c2}$  plot did not include the last two points.

## D. Si<sup>3+</sup>

The polarization plot for Si<sup>3+</sup> is shown in Figure 2. The most notable feature is the large difference between the  $\Delta E_{c1}$  and  $\Delta E_{c2}$  data-sets. The other notable feature is the pronounced deviation from linear of the  $\frac{\Delta E_{c2}}{\Delta \langle r^{-4} \rangle}$  plot.

Examination of Table VIII for the (29,8)-(29,9) interval shows that the net  $\Delta E_{7,8,8L}$  correction is very close in magnitude to the  $\Delta E_6$  energy correction. The  $\Delta E_{7,8,8L}$  correction is still more than 50% of the  $\Delta E_6$  correction for the (29,10)-(29,11) interval. The polarization series is an asymptotic series [70, 79] and is not absolutely convergent as  $n$  increases. As mentioned by Drachman [70], a condition for the usefulness of the polarization series is that the  $\Delta E_{7,8,8L}$  corrections should be significantly smaller than the  $\Delta E_6$  corrections. This condition is not satisfied for the first two intervals and leads to the noticeable curvature in the plot of the  $\Delta E_{c2}$  data points.

The resolution to this problem would be to increase the  $L$  values at which the intervals are measured. But Stark shift corrections become increasingly important at high  $L$ . The Stark shift corrections are significant for the (29,11)-(29,14) interval.

A line of best fit was drawn using the four data points with  $\Delta \langle r^{-6} \rangle / \Delta \langle r^{-4} \rangle < 0.004$ . The linear regression gave an intercept of  $B_4 = 3.7163(32)$  and a slope of  $B_6 = -30.96(134)$ . The intercept translates to a polarizability of 7.433 a.u.. To put this in perspective, the polarizability originally deduced from the RESIS experiment was 7.408(11) [4]. A later analysis which included the  $C_7$  and  $C_{8L}$  potentials gave 7.426(12) a.u. [5]. There has been a steady increase in the derived dipole polarizability as more higher-order terms in the polarization series are incorporated into the analysis.

The polarization plot  $B_6$  of  $-30.96(134)$  was about 10% larger in magnitude than the MBPT-SD value of  $-27.06(5)$ . This value of  $B_6$  results in a quadrupole polarizability of  $\alpha_2 = (-2 \times 30.96 + 6 \times 11.04) = 4.34$  a.u. which is 60% smaller than the HFCP and MBPT-SD polarizabilities. The uncertainty of  $(2 \times 1.34 + 6 \times 0.006) = 3.0$  a.u. is too small to allow consistency with the theoretical values.

### E. An alternate perspective

The analysis so far can be regarded as a standard polarization analysis but with additional refinements due to improved knowledge about the higher-order terms in the polarization series. However, it is worthwhile to examine the analysis from a different perspective.

The comparison between first principles theory and the RESIS experiment has resulted in agreement to better than 1% for dipole polarizabilities. The quality of the agreement for the quadrupole polarizability is not nearly so good. But can the analysis of the RESIS experiment be expected to yield quadrupole polarizabilities that are a serious test of calculation? The quadrupole polarizability is derived from the slope of the polarization plot. But the higher-order polarization corrections and Stark shifts result in energy corrections that amount to between 30-100% of the raw  $C_6$  energy shift. And it must be recalled that the polarization series itself is an asymptotic series [79] so there are uncertainties about the size of omitted terms.

One way forward is to use the dipole polarizability comparison as a guide to the accuracy of the quadrupole polarizability. The first principles dipole polarizabilities are expected to be accurate to better than 0.5% and this has been confirmed by experiment. As discussed earlier, the uncertainty in the quadrupole polarizability for Na-like ions should be smaller than the dipole polarizability. Therefore it is not credible to postulate large errors in the atomic structure calculations of the quadrupole polarizability on the basis of a  $B_6$  derived from the polarization plot. It makes more sense to use the theoretical  $C_6$  to estimate the size of unaccounted systematic effects in the measured energy shifts.

The large uncertainties in  $B_6$  do not detract greatly from the the accuracy of the dipole polarizability. One of the reasons higher-order effects can substantially impact  $B_6$  is that  $\Delta E_6$  is small because of the cancellation between  $\alpha_2$  and  $\beta_1$ . However, the relatively small size of  $B_6$  means a large uncertainty in  $B_6$  has a relatively small impact on the derived  $\alpha_1$ .

The impact of possible systematic errors on  $\text{Mg}^+$  was determined by redoing the linear regression with a fixed value of  $B_6$  that was constrained to lie between  $-251.2 \pm 19.0$ . The uncertainty of 19.0 was derived by adding the statistical uncertainty of 7.9 from the initial linear regression fit to  $|240.1 - 251.2|$ , the difference between the  $C_6$  of Table VII and the initial  $B_6$  from the linear regression. This gave a revised uncertainty of  $\delta B_4 = 0.015$ , leading to a final  $\alpha_1$  of 35.04(3) a.u..

The same analysis was repeated for  $\text{Si}^{3+}$ . In this instance the derived value of  $\alpha_1$  was 7.433(25) a.u..

### F. Estimate of the resonant oscillator strengths.

As the polarizabilities are dominated by the resonant transition it is possible to derive an estimate for the resonant multiplet strength [80]. We use the relation

$$S_{3s-3p} = \frac{\frac{\alpha_1 - \alpha'_1 - \alpha_{\text{core}}}{2}}{\frac{9\Delta E_{3s-3p_{1/2}}}{4}} + \frac{\frac{\alpha_1 - \alpha'_1 - \alpha_{\text{core}}}{4}}{9\Delta E_{3s-3p_{3/2}}} . \quad (29)$$

In this expression  $\alpha_1$  is the polarizability extracted from the polarization plot while  $\alpha_{\text{core}}$  is the net core polarizability, and  $\alpha'_1$  is the valence polarizability excluding the resonant transition. For the  $\text{Mg}^+$  multiplet, we use

$$S_{3s-3p} = \frac{35.044 - 0.112 - 0.463}{4.08436} = 8.439 . \quad (30)$$

Using the uncertainties detailed earlier, the final value is 8.439(11). This is equivalent to a line strength of  $S_{3s-3p_{3/2}} = 11.25(2)$ , in agreement with the recent experimental value of 11.24(6) [50].

Repeating the analysis for  $\text{Si}^{3+}$  gave a multiplet strength of 3.519(16) for the  $3s \rightarrow 3p$  transition. This is equivalent to  $S_{3s-3p_{3/2}} = 4.693(24)$  which is 0.14% larger than the MBPT-SD line strength of 4.686.

## VI. CONCLUSIONS

A survey of polarization parameters of the  $\text{Mg}^+$  and  $\text{Si}^{3+}$  ion states relevant to the analysis of the RESIS experiments by the Lundeen group [4, 5, 6] have been presented by two complementary approaches. The reanalysis of the fine-structure intervals gave dipole polarizabilities of 35.04(4) a.u. for  $\text{Mg}^+$  and 7.433(25) a.u. for  $\text{Si}^{3+}$ . The HFCEP and MBPT-SD calculations give polarizabilities that lie within 0.2% of each other for  $\text{Mg}^+$  and 0.3% for  $\text{Si}^{3+}$ . The *ab-initio* MBPT-SD dipole polarizabilities of 35.05(12) and 7.419(16) a.u. respectively agree with the experimental dipole polarizabilities to accuracy of better than 0.3%.

One notable feature of the present analysis is the very good agreement between the HFCP and MBPT-SD calculations. Indeed, the MBPT-SD calculation agrees better with the computationally simple HFCP calculation, than it does with two very large CI type calculations. For example, the polarizabilities of the completely ab-initio CI calculation [13] are about 1.5% larger than the MBPT-SD and HFCP polarizabilities. We conclude that a semi-empirical calculation based on a HF core can easily be superior to a pure CI calculation unless the CI calculation is of very large dimension. The HFCP approach has the advantage of tuning the model energy levels to experiment and this goes a long way to ensuring that many of the interesting observables will be predicted accurately. There is one feature common to the HFCP and MBPT-SD approaches. Both approaches approximate the physics of the dynamical corrections beyond HF/DF, but within those approximations an effectively exact calculation is made.

There are two major sources of systematic error that can impact the interpretation of the RESIS experiment. To a certain extent one has to choose the  $(n, L)$  states to navigate between the Scylla [81] of non-adiabatic corrections and the Charybdis [81] of Stark shifts. If  $L$  is too small, then the  $\Delta E_{7,8,L}$  shift becomes larger than  $\Delta E_6$ , thus invalidating the use of Eq. (1). On the other hand, Stark shift corrections become increasingly bigger as  $L$  becomes larger. These problems are most severe in  $\text{Si}^{3+}$  and are responsible for the slope of the polarization curve being different from the atomic structure predictions. An explicit two-state model of long range polarization interactions is probably needed to realize the full potential of the RESIS experiment

## Acknowledgments

This work was supported in part by the National Science Foundation Grant No. PHY-0758088.

- 
- [1] S. R. Lundeen, Adv. At. Mol. Opt. Phys. **52**, 161 (2005).
  - [2] R. J. Drachman, Phys. Rev. A **26**, 1228 (1982).
  - [3] R. J. Drachman and A. K. Bhatia, Phys. Rev. A **51**, 2926 (1995).

- [4] R. A. Komara, M. A. Gearba, S. R. Lundeen, and C. W. Fehrenbach, *Phys. Rev. A* **67**, 062502 (2003).
- [5] E. L. Snow and S. R. Lundeen, *Phys. Rev. A* **75**, 062512 (2007).
- [6] E. L. Snow and S. R. Lundeen, *Phys. Rev. A* **77**, 052501 (2008).
- [7] W. Müller, J. Flesch, and W. Meyer, *J. Chem. Phys.* **80**, 3297 (1984).
- [8] J. Mitroy, D. C. Griffin, D. W. Norcross, and M. S. Pindzola, *Phys. Rev. A* **38**, 3339 (1988).
- [9] J. Mitroy and M. W. J. Bromley, *Phys. Rev. A* **68**, 062710 (2003).
- [10] M. S. Safronova, A. Derevianko, and W. R. Johnson, *Phys. Rev. A* **58**, 1016 (1998).
- [11] M. S. Safronova, W. R. Johnson, and A. Derevianko, *Phys. Rev. A* **60**, 4476 (1999).
- [12] M. S. Safronova and W. R. Johnson, *Adv. At. Mol. Opt. Phys.* **55**, 191 (2008).
- [13] L. Hamonou and A. Hibbert, *J. Phys. B* **40**, 3555 (2007).
- [14] P. Gill, *Metrologia* **42**, 125 (2005).
- [15] X. Baillard, M. Fouché, R. Le Targat, P. G. Westergaard, A. Lecallier, F. Chapelet, M. Abgrall, G. D. Rovera, P. Laurent, P. Rosenbusch, et al., *European Physical Journal D* **48**, 11 (2008), arXiv:0710.0086.
- [16] G. K. Campbell, A. D. Ludlow, S. Blatt, J. W. Thomsen, M. J. Martin, M. H. G. de Miranda, T. Zelevinsky, M. M. Boyd, J. Ye, S. A. Diddams, et al., *ArXiv e-prints* **804** (2008), 0804.4509.
- [17] S. A. Diddams, T. Udem, J. C. Bergquist, E. A. Curtis, R. E. Drullinger, L. Hollberg, W. M. Itano, W. D. Lee, C. W. Oates, K. R. Vogel, et al., *Science* **293**, 825 (2001).
- [18] A. Bauch, *Meas. Sci. Technol.* **14**, 1159 (2003).
- [19] V. G. Pal'chikov, Y. S. Domnin, and A. V. Novoselev, *J. Opt. B: Quantum Semiclass. Opt.* **5**, S131 (2003).
- [20] S. G. Porsev and A. Derevianko, *Phys. Rev. A* **74**, 020502(R) (2006).
- [21] T. Zelevinsky, M. M. Boyd, A. D. Ludlow, S. M. Foreman, S. Blatt, T. Ido, and J. Ye, *Hyperfine Int.* **174**, 55 (2007).
- [22] T. Rosenband, C. W. Hume, D. B. Chou, A. Brusch, L. Lorini, W. H. Oskay, R. E. Drullinger, T. M. Fortier, J. E. Stalnaker, S. A. Diddams, W. C. Swann, et al., *Science* **319**, 1808 (2008).
- [23] W. M. Itano, J. C. Bergquist, A. Brusch, S. A. Diddams, T. M. Fortier, T. P. Heavner, L. Hollberg, D. B. Hume, S. R. Jefferts, L. Lorini, et al., *Proc. SPIE* **6673**, 667303/1 (2007).
- [24] B. Arora, M. S. Safronova, and C. W. Clark, *Phys. Rev. A* **76**, 064501 (2007).
- [25] J. Mitroy and J. Y. Zhang, *Eur. Phys. J D* **46**, 415 (2008).



- [26] E. J. Angstmann, V. A. Dzuba, and V. V. Flambaum, Phys. Rev. Lett. **97**, 040802 (2006).
- [27] E. L. Snow and S. R. Lundeen, Phys. Rev. A **76**, 052505 (2007).
- [28] W. D. Robb, M. R. Meadows, T. Burnett, and G. Dollen, Phys. Rev. A **15**, 1063 (1974).
- [29] F. W. King, J. Molec. Struct. **400**, 7 (1997).
- [30] J. Mitroy and M. W. J. Bromley, Phys. Rev. A **68**, 052714 (2003).
- [31] J. Mitroy, J. Phys. B **26**, 2201 (1993).
- [32] M. W. J. Bromley and J. Mitroy, Phys. Rev. A **65**, 062505 (2002).
- [33] J. Mitroy and M. W. J. Bromley, Phys. Rev. A **68**, 035201 (2003).
- [34] J. Mitroy, Aust. J. Phys. **52**, 973 (1999).
- [35] W. R. Johnson, D. Kolb, and K. Huang, At. Data Nucl. Data Tables **28**, 333 (1983).
- [36] S. Hameed, A. Herzenberg, and M. G. James, J. Phys. B **1**, 822 (1968).
- [37] S. Hameed, J. Phys. B **5**, 746 (1972).
- [38] N. Vaeck, M. Godefroid, and C. Froese Fischer, Phys. Rev. A **46**, 3704 (1992).
- [39] G. E. Brown and D. Ravenhall, Proc. R. Soc. London, Ser. A **208**, 552 (1951).
- [40] W. R. Johnson, S. A. Blundell, and J. Sapirstein, Phys. Rev. A **37**, 307 (1988).
- [41] S. A. Blundell, W. R. Johnson, and J. Sapirstein, Phys. Rev. A **43**, 3407 (1991).
- [42] W. R. Johnson, Z. W. Liu, and J. Sapirstein, At. Data and Nuclear Data Tables **64**, 279 (1996).
- [43] Y. Ralchenko, A. Kramida, J. Reader, and NIST ASD Team, *NIST Atomic Spectra Database Version 3.1.5* (2008), URL <http://physics.nist.gov/asd3>.
- [44] U. Volz and H. Schmoranzer, Phys. Scr. **T65**, 48 (1996).
- [45] U. Volz, M. Majerus, H. Liebel, A. Schmitt, and H. Schmoranzer, Phys. Rev. Lett. **76**, 2862 (1996).
- [46] E. Tiemann, H. Knockel, and H. Richling, Z. Phys. D **37**, 323 (1996).
- [47] K. M. Jones, P. S. Julienne, P. D. Lett, W. D. Phillips, E. Tiesinga, and C. J. Williams, Europhys. Lett. **35**, 85 (1996).
- [48] C. W. Oates, K. R. Vogel, and J. L. Hall, Phys. Rev. Lett. **76**, 2866 (1996).
- [49] W. Ansbacher, Y. Li, and E. H. Pinnington, Phys. Lett. A **139**, 165 (1989).
- [50] M. Hermann, V. Batteiger, S. Knunz, G. Saathoff, T. Udem, and T. W. Hansch (2008), arXiv:physics/0808:4061v1.
- [51] H. G. Berry, J. Bromander, and R. Buchta, Phys. Scr. **181**, 125 (1970).

- [52] J. Kernahan, E. H. Pinnington, J. A. O'Neill, R. L. Brooks, and K. E. Donnelly, *Phys. Scr.* **19**, 267 (1979).
- [53] Y. Baudinet-Robinet, P. D. Dumont, H. P. Garnir, E. Biemont, and N. Grevesse, *J. de. Physique Colloque C1* **40**, C1 (1979).
- [54] S. T. Maniak, E. Träbert, and L. J. Curtis, *Phys. Letters A* **173**, 407 (1993).
- [55] B. J. Lyons and T. F. Gallagher, *Phys. Rev. A* **57**, 2426 (1998).
- [56] C. E. Theodosiou, L. J. Curtis, and C. A. Nicolaides, *Phys. Rev. A* **52**, 3677 (1995).
- [57] S. Sahoo, *Chem. Phys. Lett.* **448**, 144 (2007).
- [58] J. Y. Zhang and J. Mitroy, *Phys. Rev. A* **76**, 022705 (2007).
- [59] B. M. W. J. Mitroy, J and K. Rollin, **0**, under review (2008).
- [60] C. Froese Fischer, G. Tachiev, and A. Irimia, *At. Data Nucl. Data Tables* **92**, 607 (2006).
- [61] B. W. Shore and D. H. Menzel, *Principles of Atomic Spectra* (John Wiley and Sons, New York, 1968).
- [62] U. Fano and J. W. Cooper, *Rev. Mod. Phys.* **40**, 441 (1968).
- [63] U. J. Sofia, D. Fabian, and J. C. Howk, *Astrophys. J* **531**, 384 (2000).
- [64] E. L. Fitzpatrick, *Astrophys. J Lett.* **482**, L199 (1997).
- [65] S. G. Porsev and A. Derevianko, *JETP* **129**, 227 (2006).
- [66] J. Mitroy and J. Y. Zhang, *Phys. Rev. A* **76**, 032706 (2007).
- [67] J. Mitroy and J. Y. Zhang, *Phys. Rev. A* **76**, 062703 (2007).
- [68] M. S. Safronova, C. J. Williams, and C. W. Clark, *Phys. Rev. A* **69**, 022509 (2004).
- [69] J. Mitroy and M. W. J. Bromley, *Phys. Rev. A* **70**, 052503 (2004).
- [70] R. J. Drachman, *Can. J. Phys.* **60**, 494 (1982).
- [71] A. Kumar and W. J. Meath, *Can. J. Chem.* **60**, 1616 (1985).
- [72] R. R. Freeman and D. Kleppner, *Phys. Rev. A* **14**, 1614 (1976).
- [73] H.-J. Werner and W. Meyer, *Phys. Rev. A* **13**, 13 (1976).
- [74] G. Maroulis and A. J. Thakkar, *Chem. Phys. Lett.* **156**, 87 (1989).
- [75] A. Nicklass, M. Dolg, H. Stoll, and H. Preuss, *J. Chem. Phys.* **102**, 8942 (1995).
- [76] K. Bockasten, *Phys. Rev. A* **9**, 1087 (1974).
- [77] B. Edlen, *Handbuch der Physik*, vol. 27 (Springer-Verlag, Berlin, 1964).
- [78] G. W. F. Drake and R. A. Swainson, *Phys. Rev. A* **44**, 5448 (1991).
- [79] A. Dalgarno and J. T. Lewis, *Proc. Phys. Soc. London Ser. A* **69**, 57 (1956).

- [80] M. S. Safronova and C. W. Clark, Phys. Rev. A **69**, 040501(R) (2004).
- [81] Homer, *The Odyssey* (circa 900BC).

TABLE I: Theoretical and experimental energy levels (in Hartree) of some of the low-lying states of the  $\text{Mg}^+$  and  $\text{Si}^{3+}$  ions. The energies are given relative to the energy of the  $\text{Mg}^{2+}$  and  $\text{Sr}^{4+}$  cores. The experimental energies are taken from the National Institute of Standards and Technology database [43]. The HFCP energies should be interpreted as the  $J$  weighted average of the spin-orbit doublet.

State	Experiment	MBPT-SD	HFCP
$\text{Mg}^+$			
$3s_{1/2}$	-0.552536	-0.552522	-0.552536
$3p_{1/2}$	-0.390015	-0.390030	-0.389737
$3p_{3/2}$	-0.389597	-0.389611	
$4s_{1/2}$	-0.234481	-0.234470	-0.234323
$3d_{5/2}$	-0.226803	-0.226772	-0.226804
$3d_{3/2}$	-0.226799	-0.226768	
$4p_{1/2}$	-0.185206	-0.185210	-0.185014
$4p_{3/2}$	-0.185067	-0.185071	
$4d_{5/2}$	-0.127382	-0.127374	-0.127373
$4d_{3/2}$	-0.127379	-0.127372	
$\text{Si}^{3+}$			
$3s_{1/2}$	-1.658930	-1.658973	-1.658928
$3p_{1/2}$	-1.334120	-1.334094	-1.332738
$3p_{3/2}$	-1.332019	-1.331999	
$3d_{5/2}$	-0.928210	-0.928138	-0.928302
$3d_{3/2}$	-0.928205	-0.928134	
$4s_{1/2}$	-0.775097	-0.775104	-0.774681
$4p_{1/2}$	-0.664433	-0.664421	-0.663640
$4p_{3/2}$	-0.663696	-0.663684	
$4d_{5/2}$	-0.519810	-0.519800	-0.519743
$4d_{3/2}$	-0.519809	-0.519799	
$4f_{5/2}$	-0.501044	-0.501044	-0.501033
$4f_{7/2}$	-0.501032	-0.501035	

TABLE II: Line strengths (in a.u.) for the resonance transitions of Na,  $\text{Mg}^+$ ,  $\text{Al}^{2+}$  and  $\text{Si}^{3+}$ . Experimental values with citations are also given. The MBPT-SD results for Na and  $\text{Al}^{2+}$  are taken from [10].

Transition	HFCP	MBPT-SD	BSR-CI	Experiment
$\text{Na}$				
$S_{3s-3p_{1/2}}^{(1)}$	12.44	12.47	12.60	12.412(16) [44, 45] 12.435(41) [46]
$S_{3s-3p_{3/2}}^{(1)}$	24.88	24.94	25.20	24.876(24) [47] 24.818(34) [44, 45] 24.844(54) [48]
$\text{Mg}^+$				
$S_{3s-3p_{1/2}}^{(1)}$	5.602	5.612	5.644	5.645(44) [49]
$S_{3s-3p_{3/2}}^{(1)}$	11.20	11.23	11.29	11.33(12) [49] 11.24(6) [50]
$\text{Al}^{2+}$				
$S_{3s-3p_{1/2}}^{(1)}$	3.398	3.404	3.422	3.01(29) [51] 3.11(15) [52] 3.31(35) [53]
$S_{3s-3p_{3/2}}^{(1)}$	6.796	6.817	6.851	6.02(57) [51] 6.35(45) [52]
$\text{Si}^{3+}$				
$S_{3s-3p_{1/2}}^{(1)}$	2.333	2.341	2.350	2.35(10) [54]
$S_{3s-3p_{3/2}}^{(1)}$	4.666	4.686	4.707	4.70(20) [54]

TABLE III: Line strengths (in a.u.) for various transitions of  $\text{Mg}^+$  and  $\text{Si}^{3+}$ . The line strengths are mainly for dipole transitions with the exception of the  $3s \rightarrow 3d$  and  $3s \rightarrow 4d$  transitions.

Transition	$\text{Mg}^+$			$\text{Si}^{3+}$		
	HFCP	MBPT-SD	BSR-CI	HFCP	MBPT-SD	BSR-CI
$S_{3s-4p_{1/2}}^{(1)}$	0.00251	0.00261	0.00211	0.0382	0.0385	0.0385
$S_{3s-4p_{3/2}}^{(1)}$	0.00501	0.00460	0.00362	0.0764	0.0744	0.0738
$S_{3s-5p_{1/2}}^{(1)}$	0.00395	0.00402	0.00366	0.0138	0.0139	0.0138
$S_{3s-5p_{3/2}}^{(1)}$	0.00790	0.00763	0.00692	0.0276	0.0270	0.0268
$S_{3p_{1/2}-4s}^{(1)}$	2.887	2.868	2.886	0.6410	0.6334	0.6328
$S_{3p_{3/2}-4s}^{(1)}$	5.773	5.779	5.815	1.282	1.284	1.283
$S_{3p_{1/2}-5s}^{(1)}$		0.2117	0.2115		0.0633	0.0629
$S_{3p_{3/2}-5s}^{(1)}$		0.4247	0.4243		0.1284	0.1267
$S_{3p_{1/2}-3d_{3/2}}^{(1)}$	17.32	17.29	17.35	5.923	5.933	5.955
$S_{3p_{3/2}-3d_{3/2}}^{(1)}$	3.463	3.468	3.482	1.185	1.190	1.195
$S_{3p_{3/2}-3d_{5/2}}^{(1)}$	31.17	31.21	31.33	10.66	10.71	10.75
$S_{3p_{1/2}-4d_{3/2}}^{(1)}$	0.4100	0.4168	0.4631	0.0234	0.0212	0.0204
$S_{3p_{3/2}-4d_{3/2}}^{(1)}$	0.0820	0.0825	0.0918	0.00468	0.00455	0.00438
$S_{3p_{3/2}-4d_{5/2}}^{(1)}$	0.7380	0.7423	0.8291	0.0421	0.0410	0.0395
$S_{3s-3d_{3/2}}^{(2)}$	97.52	97.51		16.81	16.85	
$S_{3s-3d_{5/2}}^{(2)}$	146.3	146.3		25.21	25.27	
$S_{3s-4d_{3/2}}^{(2)}$	3.615	3.638		0.2732	0.2659	
$S_{3s-4d_{5/2}}^{(2)}$	5.422	5.455		0.4098	0.3986	

TABLE IV: The polarizabilities for the  $3s$ ,  $3p$  and  $3d$  states of  $\text{Mg}^+$  and  $\text{Si}^{3+}$ . The tensor polarizabilities are for the  $M_J = J$  states. For states with  $\ell > 0$ , the MBPT-SD average values represent the weighted values for the spin-orbit doublet.

State	$\alpha_1$ (au)		$\alpha_{1,2JJ}$ (au)		$\alpha_2$ (au)		$\alpha_3$ (au)	
	HFCP	MBPT-SD	HFCP	MBPT	HFCP	MBPT-SD	HFCP	MBPT-SD
$\text{Mg}^+(3s)$	34.99	35.05	0	0	156.1	156.1	1715	1719
$\text{Mg}^+(3p_{1/2})$		31.60	0	0		340.2		11778
$\text{Mg}^+(3p_{3/2})$		31.88	1.162	1.156		343.0		11879
$\text{Mg}^+(3p - \text{Average})$	31.79	31.79			341.7	342.1	11839	11845
$\text{Mg}^+(3d_{3/2})$		189.3	-78.47	-79.15		-9336		$2.857 \times 10^5$
$\text{Mg}^+(3d_{5/2})$		188.6	-112.1	-112.2		-9341		$2.860 \times 10^5$
$\text{Mg}^+(3d - \text{Average})$	189.5	188.9			-9611	-9339	$2.855 \times 10^5$	$2.859 \times 10^5$
$\text{Si}^{3+}(3s)$	7.399	7.419	0	0	12.13	12.15	47.03	47.15
$\text{Si}^{3+}(3p_{1/2})$		3.120	0	0		13.05		155.1
$\text{Si}^{3+}(3p_{3/2})$		3.183	1.459	1.462		13.21		157.1
$\text{Si}^{3+}(3p - \text{Average})$	3.158	3.162			13.17	13.16	156.3	156.5
$\text{Si}^{3+}(3d_{3/2})$		5.168	-0.6083	-0.631		58.61		695.2
$\text{Si}^{3+}(3d_{5/2})$		5.131	-0.8690	-0.848		58.61		696.2
$\text{Si}^{3+}(3d - \text{Average})$	5.135	5.146			58.43	58.61	693.2	695.8

TABLE V: Breakdown of the different contributions to the dipole polarizabilities of  $\text{Mg}^+$  and  $\text{Si}^{3+}$ . The  $\epsilon p$  contribution includes both pseudo-state and continuum states. Dipole polarizabilities from other sources are also listed with citation. The estimated uncertainties for the different components of the uncertainty as estimated in brackets. The RESIS reanalysis are taken from the reanalysis of the RESIS fine-structure intervals described later.

Quantity	$\text{Mg}^+$		$\text{Si}^{3+}$	
	HFCP	MBPT-SD	HFCP	MBPT-SD
$3s \rightarrow 3p$	34.413	34.478(100)	7.153	7.180(6)
$3s \rightarrow (4-6)p$	0.021	0.020(0)	0.054	0.053(0)
$3s \rightarrow \epsilon p$	0.091	0.087(4)	0.030	0.029(1)
Core	0.481	0.481(10)	0.162	0.162(8)
Core-Valence	-0.018	-0.018(2)	-0.005	-0.005(1)
Total	34.99	35.05(12)	7.394	7.419(16)
CI [13]	35.66		7.50	
RESIS [5, 6]	35.00(5)		7.426(12)	
Laser Exp [55]	33.80(50)			
$f$ -sums [56]	35.1			
RCC [57]	35.04			
RESIS reanalysis	35.04(3)		7.433(25)	



TABLE VI: Breakdown of the different contributions to the quadrupole polarizabilities of  $\text{Mg}^+$  and  $\text{Si}^{3+}$ . The  $\epsilon p$  contribution includes both pseudo-state and continuum states. The quadrupole polarizabilities from a RESIS analysis is listed.

Quantity	$\text{Mg}^+$		$\text{Si}^{3+}$	
	HFCP	MBPT-SD	HFCP	MBPT-SD
$3s \rightarrow 3d$	149.69	149.68(32)	11.502	11.529(9)
$3s \rightarrow (4-6)d$	4.99	5.01(4)	0.240	0.235(0)
$3s \rightarrow \epsilon d$	0.86	0.85(6)	0.289	0.280(8)
Core	0.52	0.52(6)	0.102	0.102(12)
Total	156.1	156.1(5)	12.13	12.15(3)
RESIS [5, 6]	222(54)			
RCC [57]	156.0			

TABLE VII: The polarizabilities and  $C_n$  parameters computed from the composite list of HF/CP and MBPT-SD matrix elements. The parameters tabulated here can be regarded as the recommended theoretical values. The  $C_7$ ,  $C_8$  and  $C_{8L}$  parameters were used in the analysis the RESIS spectra for  $\text{Mg}^+$  and  $\text{Si}^{3+}$ .

Quantity	$\text{Mg}^+$	$\text{Si}^{3+}$
$\alpha_1$	35.05(12)	7.419(16)
$\alpha_2$	156.1(5)	12.15(3)
$\alpha_3$	1715(6)	47.03(12)
$\beta_1$	106.0(3)	11.04(1)
$\beta_2$	236.1(5)	8.065(6)
$\gamma_1$	324.7(9)	16.82(1)
$\alpha_{112}$	2416(52)	89.74(41)
$\alpha_{1111}$	3511(90)	51.19(28)
$C_4$	17.53(6)	3.710(8)
$C_6$	-240.1(12)	-27.06(4)
$C_7$	-1727(27)	-125.6(2)
$C_8$	10672(92)	553.1(6)
$C_{8L}$	1169(3)	60.54(5)

TABLE VIII: Various energy corrections (in units of MHz) for the  $n = 17$  intervals of  $\text{Mg}^+$  and the  $n = 29$  intervals of  $\text{Si}^{3+}$ . These were computed using  $C_n$  values of Table VII.

$n$	$L_1$	$L_2$	$\Delta E_{\text{rel}}$	$\Delta E_4$	$\Delta E_6$	$\Delta E_7$	$\Delta E_8$	$\Delta E_{8\text{L}}$	$\Delta E_{\text{sec}}$	$\Delta E_{\text{ss}}$
$\text{Mg}^+$										
17	6	7	0.7314	1555.7935	-53.7751	-20.4880	7.1989	31.5551	8.1506	-0.1122
17	7	8	0.5593	678.8962	-12.6733	-3.4612	0.8512	4.9308	1.5012	-0.1702
17	8	9	0.4416	326.8907	-3.5557	-0.7292	0.1327	0.9816	0.3393	-0.2320
17	9	10	0.3575	169.8765	-1.1373	-0.1808	0.0253	0.2325	0.0896	-0.2723
17	10	11	0.2953	93.8138	-0.4026	-0.0508	0.0056	0.0627	0.0267	-0.3039
$\text{Si}^{3+}$										
29	8	9	7.2052	1172.2322	-67.1286	-27.9320	11.3800	83.6138	2.4220	-0.1658
29	9	10	5.8328	614.9317	-22.2670	-7.2876	2.3124	21.0913	0.6574	-0.3049
29	10	11	4.8184	343.2123	-8.2257	-2.1728	0.5526	6.1258	0.2026	-0.4199
29	11	12	4.0474	201.5328	-3.3152	-0.7211	0.1502	1.9896	0.0693	-0.6026
29	11	13	7.4953	324.9889	-4.7508	-0.9824	0.1956	2.6972	0.0951	-1.3540
29	11	14	10.4675	403.3750	-5.4110	-1.0843	0.2106	2.9685	0.1054	-2.3123